Enhanced iceberg discharge in the western North Atlantic during all Heinrich events of the last glaciation

Yuxin Zhou[1,2] and Jerry F. McManus[1,2]

[1]Lamont-Doherty Earth Observatory of Columbia University, Palisades, NY 10964, USA

[2]Dept of Earth and Environmental Sciences, Columbia University, New York, NY 10027, USA

Correspondence:

Yuxin Zhou

yzhou@ldeo.columbia.edu

Abstract

A series of catastrophic iceberg discharges termed Heinrich events punctuated the last ice age in the North Atlantic. During Heinrich events, coarse terrigenous debris released from the drifting icebergs and preserved in deep-sea sediments serves as an indicator of their passage. Quantifying the vertical flux of ice-rafted debris (IRD) in pelagic sediments can resolve questions regarding the timing and variation in ice sheet calving intensity. In this study, $^{230}Th_{xs}$-based IRD flux was measured throughout the last glacial period in a deep-sea sediment core from the western North Atlantic (EW9303-37JPC, 43.68°N, 46.28°W, 3981 m, EW37JPC hereafter), and complemented during Marine Isotope Stages (MIS) 1-3 by measurements from DY081-GVY001 (50.16°N, 45.51°W, 3721m, DY001GVY hereafter) in the Labrador Sea. The cores are downstream from the Hudson Strait, a leading candidate for the conduit of the icebergs from the Laurentide ice sheet (LIS). We compare our results with the directly equivalent existing data in the eastern North Atlantic, and show that EW37JPC and DY001GVY have higher IRD fluxes during all

Heinrich events, notably including 3 and 6. This study demonstrates that the Laurentide played a role in all Heinrich events and raises the likelihood that a single mechanism can account for their genesis.

Keywords: Heinrich event; western North Atlantic; IRD flux; thorium normalization

1. Introduction

The long-term climatic deterioration during the last glaciation was characterized by two types of abrupt/millennial-scale climate change. The classic Greenland ice core records document Dansgaard-Oeschger (D-O) events, rapid shifts in air temperature over the ice cap of ~8 °C within a few decades (Dansgaard et al., 1993; Grootes et al., 1993; Johnsen et al., 1992; NGRIP members, 2004). Throughout the same interval, subpolar North Atlantic deep-sea sediments preserve evidence of Heinrich events, century-scale episodes of catastrophic discharge of icebergs, represented by multiple layers of detrital sediment initially entrained in drifting icebergs, ice-rafted debris (IRD), and subsequently deposited within glacial sediment sequences (Bond et al., 1992; Broecker et al., 1992; Heinrich, 1988; Hemming, 2004).

The icebergs discharged during Heinrich events drifted and melted across the subpolar North Atlantic Ocean, an important region of deep-water formation that is sensitive to disruption by surface freshening (Manabe and Stouffer, 1997; Rahmstorf, 1995). Indeed, the associated fresh water flux may have dramatically weakened the Atlantic Meridional Overturning Circulation (AMOC) repeatedly (Henry et al., 2016; McManus et al., 2004). As a result, the Northern Hemisphere cooled (Bard et al., 2000; Bond et al., 1993) while the Southern Hemisphere warmed (Barker et al., 2009; Buizert et al., 2018). Heinrich events thus exemplify the interconnectedness of the ocean, ice, and atmosphere, highlighting the potential value their study holds for deciphering how abrupt climate change unfolds.

An unsolved mystery of the Heinrich events is the apparently anomalous behavior associated with Heinrich events 3 and 6. The two events are often regarded as the atypical Heinrich events because of their relatively low IRD concentration and lack of detrital carbonates in the eastern subpolar North Atlantic (Broecker et al., 1992). In this paper we will refer to the other Heinrich events, H 1, 2, 4, and 5, as the typical Heinrich events. The observed differences in the events have been explained by changes in the ocean or the cryosphere. This debate is relevant to understanding the mechanism(s) accounting for these dramatic events. Similar behavior of the events would fit more easily into a single mechanism, while the observed contrasts in behavior suggest different, even drastically divergent, mechanisms or causes at different times. From the glaciological point of view, Heinrich events 3 and 6 have been argued to have a European ice sheet origin from provenance studies, leading to smaller iceberg fluxes in the western North Atlantic (Grousset et al., 2000, 1993; Peck et al., 2007; Snoeckx et al., 1999), although this claim has also been disputed (Jullien et al., 2006). Furthermore, it was hypothesized that the two events occurred at the onset of the Marine Isotope Stage (MIS) 2 and 4 when the Laurentide ice sheet was just starting to grow, resulting in the smaller magnitude of calving (Gwiazda et al., 1996). On the ocean side, assuming that all the events originated from the Laurentide ice sheet, it was postulated that warmer sea surface temperatures (SST) might have melted the icebergs closer to their source in the west during the two abnormal Heinrich events (Bond et al., 1992). Consistent with that view, Pb isotope data suggest that, in the eastern North Atlantic, the apparent IRD layers are actually foraminifera-dissolution events instead (Gwiazda et al., 1996).

A reconstruction of the rate of deposition of IRD provides a straightforward test of these competing hypotheses. If the increased IRD concentrations in Heinrich layers 3 and 6 are solely the result of foraminifera dissolution, the IRD fluxes (deposition rate per unit area within a unit time) during these periods will not increase. If the icebergs originated and mostly melted in the west during the two events, the IRD fluxes will shift towards the west, and the fluxes might even be higher than during the other Heinrich events at those western sites if the total magnitude of calving remained the same. If the Laurentide ice sheet calving increased by a limited amount during the two events, the IRD fluxes will show a visible but smaller increase than the other events throughout the basin. Lastly, if the two events did originate from the European ice sheet, the IRD fluxes in the east should be higher than the west.

The rapid scavenging of ^{230}Th, in balance with its constant production, allows it to be used to reconstruct mass flux (Bacon, 1984; Bacon and Anderson, 1982; Bacon and Rosholt, 1982). IRD flux can be reconstructed from the ^{230}Th burial flux of sediment that is uniquely identified as IRD. Resolving the IRD fluxes during Heinrich events provides a pathway to test the aforementioned hypotheses on the two atypical events. Previously, they have only been measured in century-scale resolution in the eastern North Atlantic (McManus et al., 1998). Here we present a 135-thousand-year (kyr) ice-rafting record off the coast of Newfoundland, 2200 km downstream from the Hudson Strait. We complement it with a record from Orphan Knoll that is ~1700 km downstream from the Hudson Strait and extends through Heinrich layer 3, which may have been disturbed by turbidites in the first core. By comparing our ice-rafting records with the directly equivalent existing data in the eastern North Atlantic, we attempt to demonstrate the non-unique nature of Heinrich events 3 and 6 in the context of other Heinrich events of the last glaciation from a western North Atlantic perspective.

2. Methods

EW37JPC (43.68°N, 46.28°W, 3981 m, IGSN: DSR000507) is a 13.315-m-long jumbo piston core retrieved at the foot of a continental slope, off the coast of Newfoundland, Canada (Figure 1). DY001GVY (50°09'36''N, 45°30'36''W, 3721m) is a gravity core retrieved near Orphan Knoll (Figure 1). Both cores are today under the influence of the Labrador Current at the surface, which brings materials from the mouth of the Hudson Strait. At depth, the deep western boundary current (DWBC) flows southward past the sites (McCartney, 1992).

Samples of 8-10 g were taken at 2 cm intervals from EW37JPC and at 5 cm intervals from DY001GVY. The samples were freeze dried, weighed and washed through 63 μm sieves to separate the coarse and fine fraction. Coarse fraction (% coarse) is calculated by dividing dried >63 μm fraction weight against the total dry weight. The >150 μm fraction was split so that 300-400 foraminifera shells and ~100 IRD grains were identified and quantified under a microscope. The counting results were used to calculate the relative abundance of the polar planktic foraminifera, *Neogloboquadrina pachyderma* (hereafter % *N. pachy*.), calculated as the number of *Neogloboquadrina pachyderma* specimens in a sample divided by the total number of planktic foraminifera shells, and the relative abundance of IRD (hereafter % IRD), calculated as the number of IRD grains divided by the sum of IRD grains and planktic foraminifera shells.

During microscopic identification, eight to ten specimens of *N. pachyderma* were picked for $\delta^{18}O$ and $\delta^{13}C$ analysis in the LDEO stable isotope laboratory, using a Thermo Delta V Plus equipped with a Kiel IV individual acid-bath sample preparation device. Measurements made on standard carbonate NBS19 yield a standard deviation of 0.06% for $\delta^{18}O$ and 0.03% for $\delta^{13}C$.

Elemental intensities were measured using X-ray fluorescence (XRF) core scanner in LDEO. The intensities were calibrated with flux fusion concentration measurements from EW37JPC. Samples selected to represent the full range of XRF intensities were analyzed by flux fusion following the procedure of Murray et al. (2000).

Bulk wet density and magnetic susceptibility were obtained from a Geotek multi-sensor core logger in LDEO. Local low-density peaks were identified as cracks formed due to drying and omitted in data processing.

$^{230}Th_{xs}$, or ^{230}Th derived from the decay of ^{234}U in seawater and subsequently scavenged by adsorption onto settling particles, was measured and calculated. The calculation of $^{230}Th_{xs}$ has to consider two other processes that produce ^{230}Th in the sediments - detrital ^{230}Th and authigenic ^{230}Th. (Bacon, 1984; Costa and McManus, 2017; Francois et al., 2004, 1990).

Detrital ^{230}Th is the ^{230}Th produced from the radioactive decay of ^{238}U locked in the mineral lattices. Detrital ^{238}U can be estimated by assuming a constant detrital $^{238}U/^{232}Th$ and that all measured ^{232}Th is detrital. A range of $(^{238}U/^{232}Th)_{detrital}$ between 0.47 and 0.7 has been used by previous studies in this region (Table 1). We conducted a leaching experiment in EW37JPC to isolate the detrital uranium and thorium and determined $(^{238}U/^{232}Th)_{detrital}$ to be 0.48. We further determined from the leaching experiment the disequilibrium in $(^{230}Th/^{238}U)_{detrital}$ caused by α recoil to be 0.81 (details in Discussion).

Authigenic ^{230}Th is the ^{230}Th produced from the radioactive decay of ^{238}U that precipitated from the soluble form U(VI) to its insoluble form U(IV) in anoxic, reducing sediments (Barnes and Cochran, 1990; Klinkhammer and Palmer, 1991). It can be estimated by assuming the non-detrital portion of ^{238}U is authigenic. Here we assume seawater $^{234}U/^{238}U$ to be 1.1468 (Andersen et al., 2010).

The calculation of $^{230}Th_{xs}$ is thus

$$^{230}Th_{xs} = {}^{230}Th_{measured} - {}^{230}Th_{detrital} - {}^{230}Th_{authigenic}$$

$$= {}^{230}Th_{measured} - 0.48 * 0.81 * {}^{232}Th_{measured} - ({}^{238}U_{measured} - 0.48 * 0.81 * {}^{232}Th_{measured}) * [(1-e^{-\lambda 230t})$$

$$+ \lambda_{230}/(\lambda_{230}-\lambda_{234})(e^{-\lambda 234t} - e^{-\lambda 230t})(1.1468-1)]$$

0.48 is $(^{238}U/^{232}Th)_{detrital}$. 0.81 is $(^{230}Th/^{238}U)_{detrital}$. λ is the decay constant. 1.1468 is seawater $^{234}U/^{238}U$. t is the time of decay since deposition.

Each sample of ~100 mg was spiked, digested (Fleisher and Anderson, 1991), purified (Lao et al., 1993), and analyzed for uranium and thorium isotope activities. The last step was done on an Element Plus inductively coupled plasma mass spectrometer (ICP-MS). The conversion from raw counting data to activities has been packaged into a Python script named ThxsPy and published on https://github.com/yz3062/ThxsPy.

The values of $(^{238}U/^{232}Th)_{detrital}$ and $(^{230}Th/^{238}U)_{detrital}$ used by this study are different from most previous studies and are based on experimental results. We conducted leaching experiments throughout core EW37JPC to get at these lattice-bound isotopic ratios. Bulk samples were leached with 5mL of 1N or 3N HCl and sonicated for 20 minutes. After a 5-minute centrifuge, the supernatant was decanted. In some cases, the supernatant was filtered using 0.42 μm filters. The rest of the procedure is the same as described above for typical sediment U-Th analysis. The strength of acid and time of sonication used were shown previously to remove authigenic uranium effectively without leaching lattice-bound uranium and thorium (Robinson et al., 2008).

Cross correlation was performed on the time series of $\delta^{18}O$ of N. pachyderma and $^{230}Th_{xs}$ to find any potential lead or lag between the two. The 65 to 10 ka portions of both proxies were first extrapolated to a common time step of 500 years. The pairwise correlation was then computed for the two time series, first on their original chronology, then by offsetting the two by both positive and negative time steps. In each direction, up to 15 steps of offset were tested and the correlation coefficient calculated in each. The cross correlation was then bootstrapped 1000 times allowing sampling interval and time step to vary.

3. Chronology

The chronology of EW37JPC from modern to ~46 ka is based on radiocarbon dating. A monospecific sample of 350-400 specimens of *N. pachyderma*, the most abundant foraminifera species in this core, were picked from the >150μm fraction. These foraminifera shells were sonicated in water and ethanol to remove any fine-grained sediment, including detrital carbonate that can potentially bias the results. The radiocarbon analyses were performed at NOSAMS-WHOI facility. The calibration to calendar ages uses Marine 13 and the CALIB program (Stuiver et al., 2019). We use 400 years as the marine reservoir correction.

The chronology beyond the range of radiocarbon is determined by aligning our % *N. pachy.* with an alkenone-based SST record from MD01-2444 (Martrat et al., 2007). The polar foraminifera *N. pachyderma* lives in the coldest environment among planktic species and its abundance in EW37JPC signals low SST (Ericson, 1959). MD01-2444 (37°33.68′N, 10°08.53′W, 2637 m) is on the Iberian margin and its latitude is comparable to EW37JPC. Its chronology is based on North Greenland Ice Sheet Project (NGRIP) during the last glacial (Anderson et al., 2006; Johnsen et al., 2001; NGRIP members, 2004; Rasmussen et al., 2006) and before that, Antarctica Dome C (EPICA Community Members, 2004a; Parrenin et al., 2004). Even though the two sites sit on the opposite side of the North Atlantic basin, the prevailing westerlies and the resulting current put MD01-2444 downstream from EW37JPC, and so the temperatures at the two sites should be closely correlated during regional-scale climate changes. The advantage of aligning with this SST record instead of directly with NGRIP is twofold. First, both records reconstruct SST so the correlation does not need to consider meridional or air-sea signal propagation. Second, NGRIP stops at MIS 5e whereas the SST records extend beyond that, allowing us to align the late MIS 6 segment of our core as well.

The core chronology is corroborated with tephrochronology. We found several concentrated zones of plates of glassy, bubble-wall shards, consistent with the description of Ruddiman and Glover (1972). The shards are mostly non-existent outside of the zones. The youngest of these zones, at 70 cm, is identified Ash Zone 1. The commonly assumed age of Ash Zone 1 (12.2 cal ka BP) (Andrews and Voelker, 2018) is only 700 years apart from the radiocarbon-based age model. Ash Zone 2 is identified at 628.5 cm. The Ash Zone 2 was dated to 55.4 ka in the NGRIP record based on the GICC05 age model (Svensson et al., 2008) and 54.5 ka by Ar-Ar dating of the volcanic ash (Southon, 2004), whereas in our age model it is at 57.4 ka. Outside of these two zones, glass shard counts are also high at Heinrich event 3 and 6. We cannot rule out that the shards at Heinrich layer 3 were delivered by a gravity flow.

The chronology of DY001GVY is based on radiocarbon and tephrochronology. Radiocarbon analysis (n=7) in this core follows the same procedure as in EW37JPC, except the youngest sample at the depth of 2 cm used *G. bulloides* instead of *N. pachyderma* since not enough *N. pachyderma* can be found at that depth. Ash Zone 1 is identified at 58 cm, and we use 12.2 ka BP as its age (Andrews and Voelker, 2018).

4. Results

The age models indicate moderately high sedimentation rate in both cores: ~10 cm/kyr in EW37JPC and ~12 cm/kyr in DY001GVY (Figure 2 and Figure S1). EW37JPC captured the whole last glacial-interglacial cycle (MIS 1-5) and the very end of MIS 6. DY001GVY extends to just beyond 30 ka. Crossed beddings of foraminifera-rich sands are found in EW37JPC around depths 288 cm – near the depth where Heinrich layer 3 is found – (Figure S2) and 1312 cm. They are likely caused by turbidites and could influence the interpretation of results from this one interval. Data from Heinrich event 3 in EW37JPC is therefore considered tentatively except as it is consistent with independent evidence from DY001GVY, which is from a different location not influenced by any turbidite deposits, and has a similarly high sedimentation rate.

In EW37JPC, Heinrich layers are identified by peaks of Ca/Sr (Hodell et al., 2008), magnetic susceptibility, density, % coarse, and % IRD (Figure 3). Layers with prominent increases in all the above proxies are present in MIS 2-4 and late MIS 6. Heinrich events 4 and 5 show the strongest signal in all of these proxies, consistent with previous findings (Hemming et al., 2004). Several episodes of smaller magnitude can be found during early MIS 5. The strongest peak of Ca/Sr appears at 1220 cm depth, and is matched with a $^{230}Th_{xs}$ low. However, no signals in magnetic susceptibility, % coarse, % IRD, % *N. pachy.*, or $\delta^{18}O$ are visible at this depth (density data does not extend to this depth). This suggests the delivery of fine detrital carbonates at a high rate without fresh water flux or lower SST. A possible explanation is a gravity flow that originates from a region with high concentration of detrital carbonates. In DY001GVY, Ca/Sr, magnetic susceptibility, density, and % coarse help pin down the location of Heinrich events. Possibly due to its more poleward location and setting within the cold Labrador current, % IRD and % *N. pachy*. are saturated to 100% in this core during most of the last glacial period.

In EW37JPC, in each of the identified Heinrich events, % *N. pachy*. increased while $\delta^{18}O$ of *N. pachyd*erma decreased. The profile of % *N. pachy*. behaves differently during Heinrich events than the profile of % IRD, however, as % *N. pachy*. continues to vary even when % IRD stabilizes at a high value. $\delta^{18}O$ of *N. pachyderma* is a hybrid between the typical sawtooth glacial-interglacial cycle and episodes of depletion corresponding to Heinrich events.

Our leaching experiment on EW37JPC sediments suggests that the recoil-related losses of ^{234}U and ^{230}Th are about 10% each on average in Heinrich layer detrital sediments and higher in between (Figure S3). The variations in $^{234}U/^{238}U$ are smaller than those of $^{230}Th/^{234}U$. We use 0.9

for $^{230}Th/^{234}U$ and $^{234}U/^{238}U$ and 0.81 for $^{230}Th/^{238}U$ for both cores. The leaching experiment also suggests a potentially large range in the detrital $^{238}U/^{232}Th$ ratio (Figure 5), but the five leaching experiments made in Heinrich layer 4 have an average of 0.48, which we use in this study.

The $^{230}Th_{xs}$ profile from EW37JPC contains values that vary between 0-5 dpm/g. Low $^{230}Th_{xs}$ values (<0.5 dpm/g) are observed at 16.3, 24.0, 38.1, 45.8, 60.6, 67.8 ka during the last glacial period. The low $^{230}Th_{xs}$ episodes have ages 1 kyr within the previously determined Heinrich event ages (Hemming, 2004), which is broadly within the uncertainty of radiocarbon dating. One sample in Heinrich event 4 and another in late MIS 6 have $^{230}Th_{xs}$ so low that their 95% uncertainty range barely reach above 0. DY001GVY resembles EW37JPC in $^{230}Th_{xs}$ for the most part, except the periods before and after Heinrich event 2.

From $^{230}Th_{xs}$, we can calculate vertical mass flux

$$F = \beta * Z / {}^{230}Th_{xs,0}$$

Where F is the vertical mass flux, β is the production rate of ^{230}Th, Z is the water depth, and $^{230}Th_{xs,0}$ is $^{230}Th_{xs}$ corrected for decay since deposition using the independent age model. We can further calculate the IRD flux

IRD flux = F * #IRD / M

where #IRD is the total number of IRD grains, accounting for the splits. M is the dry bulk mass.

In EW37JPC, the IRD flux during the Heinrich event 11 and Heinrich event 5 are the highest among Heinrich events, with values at 500,000 #/cm^{2}kyr. The IRD flux during Heinrich event 2 and 4 are around 250,000 #/cm^{2}kyr. The IRD flux at Heinrich event 1, Heinrich event 6 and the event prior to Heinrich event 6 are lower at 100,000 #/cm^{2}kyr, 41,000 #/cm^{2}kyr and 42,000 #/cm^{2}kyr, respectively. The IRD fluxes during each Heinrich events and the event prior to

Heinrich event 6 are statistically distinct from the ambient IRD flux, even at the smallest event (Heinrich event 6), where the p-value of the "Student's" t Test is 4×10^{-6}. In DY001GVY, the mass flux is lower than EW37JPC. During Heinrich events 1-3, the mass fluxes are around 20-30 g/cm^2kyr. However, unlike EW37JPC, DY001GVY shows a clearer signal of mass flux increase during Younger Dryas. The IRD flux is highest during Heinrich events 1 and 2 at about 160,000 $\#/cm^2kyr$, followed by the Last Glacial Maximum at 120,000 $\#/cm^2kyr$, and Heinrich event 3 at 90,000 $\#/cm^2kyr$. A "Student's" t Test similarly shows that the Heinrich event 3 IRD flux is distinctly different from the ambient sediment (p-value=1×10^{-10}).

5. **Discussion**

5.1. Interpretation of IRD flux

Heinrich event sedimentary layers have been viewed as the possible result of intervals of decreased foraminifera productivity, foraminifera dissolution, increased IRD deposition, or some combination of those influences. Previously, the only $^{230}Th_{xs}$-based quantification of the depositional flux of grains that are uniquely identified as IRD during the Heinrich events is from V28-82 in the eastern subpolar North Atlantic (McManus et al., 1998). The results of V28-82 showed that Heinrich events 1, 2, 4, and 5 were at least in part increased ice-rafting events, but left open the question for the other two events. Our new results from EW37JPC and DY001GVY reaffirm McManus et al.'s conclusion, showing increased IRD flux for the four most typical Heinrich events (Figure 4 c). Additionally, here we show for the first time that, at least in the western North Atlantic, the sediment layers associated with the other two of the original Heinrich events, 3 and 6, were also the result of increased ice-rafted deposition, rather than solely the result of reduced productivity near the sea surface or enhanced foraminifera dissolution on the seafloor.

Numerically, V28-82 displays about half of the IRD flux of the western cores during Heinrich events 1 and 2, and about half of the IRD flux of EW37JPC during Heinrich events 4 and 5. The most dramatic differences are observed during Heinrich events 3, 6, and 11. The increases in IRD fluxes in V28-82 are very much muted during these events, whereas the IRD flux in EW37JPC during Heinrich event 3 is thirty times higher than V28-82, during Heinrich event 6 nine times higher, and during Heinrich event 11 twenty times higher. Although Heinrich event 3 in EW37JPC is very near what may be turbidite deposit, an increase in IRD flux during this interval similarly occurs in core DY001GVY, which has no evidence of turbidite deposition and records an IRD flux that is eight times higher than in V28-82. A comparison of IRD concentration and mass flux, two variables used to calculate IRD flux, reveals that much of the difference between V28-82 and the two western cores comes from the difference in mass flux, confirming that while IRD was an important sedimentary component at both locations, much more of it was deposited in the west during this interval (Figure 4 a and b).

Since the eastern core displays much lower IRD flux during Heinrich events 3 and 6, a stronger zonal flux gradient may have existed during these two periods – more icebergs melted in the western basin, with fewer icebergs reaching, and therefore less IRD deposited within, the east. The distinct melting patterns could be explained by any one, or a combination of, the following three factors: The calving flux from the Laurentide was smaller in magnitude during Heinrich events 3 and 6 so the majority of the drifting ice melted in the western NA without making it to the east; some different ice sheet(s) contributed to or dominated calving during this interval; or the surface ocean current patterns were different, causing changed iceberg trajectories.

If the calving of icebergs from the Laurentide ice sheet increased during H3 and H6 but to a lesser extent than during the other events, the IRD fluxes associated with these two would display a visible but smaller increase than in H1, H2, H4 and H5 across the subpolar Atlantic and a possible gradient from west to east. At face value, our data are consistent with this hypothesis. Heinrich events 3 and 6 do display increases in IRD flux that are smaller in magnitude than the other events, and there is a clear depositional gradient. Several hypotheses have been proposed to explain the smaller magnitude of calving during these events. Gwiazda et al. (1996) speculated that the ice sheet volume during the two events could be smaller, leading to the smaller magnitude of calving. The reasoning goes that the two events occur at the onset of the MIS 2 and 4, when the Laurentide ice sheet was just starting to regrow after periods of warmth. A similar yet distinct hypothesis stated that H4, which in our western cores appear to be a particularly large event, "gutted" the Hudson Strait ice presence and left it in an open marine setting (Kirby and Andrews, 1999). As a result, H3 occurred when the Laurentide was still in a growth phase from Ungava Bay. The lack of a signal of H3 and H6 in V28-82 to the east may also reflect the greater distance from the source of icebergs, as well as the likelihood that H3 and H6 icebergs were less dirty. The dirtiness of icebergs has been hypothesized to change among Heinrich events (Andrews, 2000; Kirby and Andrews, 1999), which would lead to differences in IRD fluxes. However, we are not aware of any evidence to suggest that H3 and H6 icebergs were different in dirtiness in particular.

It has been also suggested that Heinrich event 3 and 6 may have had a European ice sheet origin (Grousset et al., 2000, 1993; Snoeckx et al., 1999). Our data do not support an entirely European origin for Heinrich event 3 and 6, since the deposition of IRD during each was demonstrably greater in the western North Atlantic, and given the greater difficulty of European-originating icebergs to reach the western sites. The unlikeliness of this scenario is supported by an iceberg trajectory study (Death et al., 2006). We cannot rule out, however, that associated or precursor events of a European origin took place.

Our data also do not directly support the hypothesis that all the Heinrich events were characterized by a similar magnitude of iceberg discharge from the Laurentide ice sheet, but that there was greater melting in the west during Heinrich events 3 and 6 due to warmer SST or a reorganization of the circulation pattern. Although IRD fluxes increased during Heinrich events 3 and 6 at our western sites, the fluxes are not higher than during the other Heinrich events. Combined with the essential lack of increased IRD deposition at the eastern site, the total IRD flux during H3 and H6 appears to be lower compared to the other events.

IRD flux reconstruction provides an important potential constraint on modeled iceberg discharge during Heinrich events as a freshwater delivery mechanism (Death et al., 2006). Yet most Heinrich event modeling studies have focused on meltwater flux (Ganopolski and Rahmstorf, 2001; Prange et al., 2004; Roberts et al., 2014) and iceberg calving flux (Alvarez-Solas et al., 2013, 2010; Bassis et al., 2017; Marshall and Koutnik, 2006). This is a missed opportunity for meaningful data-model comparison, since the absolute values of melt water flux or iceberg calving flux are nontrivial to reconstruct with paleo proxies. Melt water proxies, including $\delta^{18}O$ (Roche et al., 2004), %C37:4 (Naafs et al., 2011; Rodrigues et al., 2017; Stein et al., 2009), and $^{10}Be/^{9}Be$ (Valletta et al., 2018), are, although valuable, only qualitative. The magnitude of iceberg calving is typically reconstructed by IRD grain concentration, which again is only qualitative (e.g. Bond et al., 1992). Therefore, IRD flux is the most accessible proxy with the potential for comparable model output. The observational community should seek to better understand the IRD entrainment mechanism, and the modeling community should incorporate the IRD delivery and deposition in simulations, which can then be compared with IRD flux reconstructions. Such comparisons can potentially help assess ice sheet calving simulations and improve the understanding of calving behaviors.

5.2.Sea surface proxies

Possibly due to its more poleward location, the relative abundance of polar foraminifera (% *N. pachy.*) from DY001GVY is saturated at 100% for most of the last glacial period (Figure 3). The % *N. pachy*. data from EW37JPC exhibits more variability and increases in every Heinrich event layer, indicating repeated sea-surface cooling. During Heinrich events 1, 2, and 4, % *N. pachy*. seems to show a double peak structure. This might suggest that the SST is lowest at the beginning and end of these Heinrich events, but briefly returned to warmer temperatures midway through the events. We do not see a similar sequence of delayed onset in the deposition of IRD after the initial increase in *N. pachyderma* abundance reported previously (Barker et al., 2015).

The $\delta^{18}O$ of *N. pachy*derma from EW37JPC displays both the typical sawtooth glacial-interglacial cycle and episodes of depletion associated with Heinrich events (Figure 3). Given the % *N. pachy*. increase and therefore implied SST decrease during Heinrich events, the depletion of $\delta^{18}O$ cannot be the result of temperature changes. The likely explanation is that the melting icebergs released a large amount of $\delta^{18}O$-depleted freshwater during each Heinrich event. The depletion of planktic $\delta^{18}O$ is less obvious in Heinrich event 6 and HQ, but it also did not become enriched during these periods. Put together with the concurrent % *N. pachy*. increases, we suggest that just like the other Heinrich events, influx of freshwater reached this site. The depletion of *N. pachyderma* $\delta^{18}O$ is consistent with previous studies on North Atlantic cores (Bond et al., 1992; Cortijo et al., 1997; Hillaire-Marcel et al., 1994; Labeyrie et al., 1999). Cortijo et al. (1997) mapped out changes in *N. pachyderma* $\delta^{18}O$ across the North Atlantic during Heinrich event 4. The magnitude of changes observed in our core during Heinrich event 4 (~1 ‰) is comparable to a nearby core from that study (1.1 ‰ at SU90-11).

A cross-correlation of *N. pachyderma* $\delta^{18}O$ and $^{230}Th_{xs}$ from EW37JPC during the period between Heinrich events 1-6 shows little lag between the two variables (Figure S4). This simultaneity is robust on a range of interpolation intervals, and does not change when the starting and ending times are varied by a few thousand years. The deposition of debris and local freshening of the sea surface were thus contemporaneous events on the time scale resolvable by our record. That is consistent with both phenomena being the direct consequence of melting icebergs, although we cannot rule out the accompanying presence of additional meltwater.

5.3. Extra events

Although Heinrich events 1-6 are the most commonly known and studied HEs of the last glacial period (e.g. Bond et al., 1992; Broecker et al., 1992; Grousset et al., 2000; Marcott et al., 2011), Heinrich (1988) postulated the existence of additional events in the early glacial and late interglacial period. A recent ice sheet modeling study (Bassis et al., 2017) predicted a previously unidentified Heinrich event which they named HQ at ~65 ka. Our IRD flux from EW37JPC provides the strongest evidence yet of the existence of HQ. In that modeling study, HQ was identified in Greenland Stadial (GS) 19. The basis of our age model is the alignment of millennial-scale cooling events (C17-C24) identified throughout the North Atlantic region (McManus et al., 1994), including on the Iberian margin (Martrat et al., 2007). There are two distinct IRD-flux events within C16 and C18, with the younger event being Heinrich event 6. It thus seems likely that the older event of the two is a good candidate to be the hypothesized event HQ. Given that Bassis et al. identified H7b prior to HQ within C19, which we identified with our % *N. pachy*. record, it is unlikely that we mistake HQ for an earlier Heinrich event. These two IRD flux events also cannot be Heinrich event 5a (Rashid et al., 2003) since we found ash zone 2 (AZ2) at a shallower depth in the core. AZ2 is between Heinrich event 5a and 6 which gives us confidence with the designation of Heinrich event 6. The fact that HQ is potentially found in EW37JPC but was absent in previous studies suggests that the influence of the event may be regionally limited, but it also raises the possibility that HQ and H6 may be mistaken for one another in previous studies. Therefore, we recommend that ocean sediment studies that seek to identify H6 or HQ should have an accompanying SST proxy to resolve cooling events C16 and C18.

During the late last interglacial period at 70, 78, 87, 105, 109, and 117 ka, we found six additional IRD flux increases from EW37JPC (Figure S5). These IRD flux increases were two orders of magnitude smaller than Heinrich events, and unlike the typical Heinrich events, changes in Ca/Sr, magnetic susceptibility, density, % coarse, % IRD, % *N. pachy*. do not accompany the IRD flux increases or have a temporal offset with the IRD flux increases. Another difference with Heinrich events is most of these IRD flux increases were preceded by discernable mass flux increases (Figure S6). This sequence of events could potentially give us a clue as to their origins. According to the turbidite-IRD sequence previously proposed to explain IRD layers in the Labrador Sea (Rashid et al., 2012), the early high mass flux could be caused by the initial melt water discharge and the ensuing turbidity and nepheloid flow. This would increase mass flux without bringing in IRD. Following the turbidite facies, IRD would have been deposited as icebergs were discharged. The number of these locally-high IRD flux events we identified correspond to the number of cooling events during the last interglacial period proposed by McManus et al. (1994), which we tentatively marked in Figure S5 and S6.

The lack of associated signals in Heinrich event proxies (Figure S5 and S6) during most of these cooling events is interesting. Among other explanations, the magnitude of the events could be too small to have detectable changes in typical Heinrich event proxies. Alternatively, the source region of the delivered materials may have changed, which could lead to the muted responses in Ca/Sr and magnetic susceptibility. It remains an open question whether these events were the result of a similar mechanism as Heinrich events but on a much smaller scale, possibly because when the Laurentide was too small to reach the coast, ice calving was less likely. These events could also be the result of meltwater outbursts, similar to the 8.2 ka event (Alley et al., 1997; Ellison et al., 2006; Keigwin et al., 2005). A third potential explanation is that they were triggered by deep turbidity currents as suggested by Hillaire-Marcel et al. (1994). Given that most of the events were associated with increases in % *N. pachy*., it is unlikely that they were caused by the deep turbidity currents alone, although a combination of the above mechanisms is still possible.

5.4. U-Th systematics

The calculation of $^{230}Th_{xs}$ commonly assumes that the detrital decay chain of ^{238}U is in secular equilibrium ($^{238}U_{det} = {}^{230}Th_{det}$). This assumption is valid when an isotopic system is closed for a sufficient length of time. However, α recoil disrupts the closed system by potentially ejecting the decay product (^{234}U or ^{230}Th in this case) or leaving it within a damaged crystal lattice site. Recently, it has been suggested that 4% of the decayed ^{234}U is lost due to α recoil, and the decay of ^{234}U further ejects 4% of ^{230}Th (Bourne et al., 2012). They reasoned that the middle value between 0.92 (1×0.96^2) and 1 (secular equilibrium), 0.96, should be used as the value of $(^{230}Th/^{238}U)_{detrital}$. Deep-sea sediments have also been observed within this range and somewhat lower (DePaolo et al., 2006). Our leaching experiment on sediments suggests that the effect of α recoil may be stronger than previously thought (Figure S3). The losses of ^{234}U and ^{230}Th are 10% each on average, although the uncertainty on ^{230}Th loss is greater. The implication of these results on calculating $^{230}Th_{xs}$ is that the detrital correction is smaller, leading to more ^{230}Th counted towards the scavenged portion and therefore higher $^{230}Th_{xs}$. This correction, compared to the equilibrium assumption, increases $^{230}Th_{xs}$ during non-Heinrich events by ~5%. Because the higher burial fluxes during Heinrich events often result in very low $^{230}Th_{xs}$, the proportional change associated with this correction is even larger (up to 70%), although the absolute change is small.

A wide range of $(^{238}U/^{232}Th)_{detrital}$ has been used in the $^{230}Th_{xs}$ calculation in the North Atlantic, ranging from 0.47 to 0.7 (Table 1). These studies use either the $^{238}U/^{232}Th$ minimum measured, which is thought to reflect the minimal influence of authigenic ^{238}U, or a vaguely defined basin-wide value. More recently, it has been suggested that $(^{238}U/^{232}Th)_{detrital}$ may vary through time (Missiaen et al., 2018). Consistent with that study's conclusion, our leaching experiment from EW37JPC (Figure 5) shows large variations in the detrital ratio as well. Since Heinrich event mass flux is the focus of this study, we choose to use the $(^{238}U/^{232}Th)_{detrital}$ that produces a conservative yet realistic estimate of mass flux throughout. The five leaching experiments made in Heinrich layer 4 provide a mean ratio of 0.48, which we use in this study. While this is toward the low end of the range of values previously applied for North Atlantic sediments, it is indeed within that range, and applying higher ratios would in some cases yield negative $^{230}Th_{xs}$, implying net sedimentary loss of ^{230}Th from settling particles to the water column, which we consider unlikely. The higher detrital ratios in other Heinrich layers could be due to the lower sampling resolution, which may not capture the lowest detrital ratios.

The relatively conservative but nonetheless very low $^{230}Th_{xs}$ results we obtained are useful to inform us that the subpolar western North Atlantic had episodically high fluxes of ice rafting, but we are hindered in using $^{230}Th_{xs}$ to normalize the burial of $^{231}Pa_{xs}$ in the form of Pa/Th as a tracer for circulation strength at this site, since the combined, propagated uncertainties on the two isotope systems at such low concentrations render the results ambiguous to the point of uninterpretable. Future studies aiming to use this approach to reconstruct rates of deep ocean circulation associated with iceberg discharges from the Laurentide should focus on sites further east or south to avoid being similarly overwhelmed by the increased IRD flux.

6. Conclusions

(1) The IRD flux in the western North Atlantic cores EW37JPC and DY001GVY increased during each Heinrich event during the last glacial cycle.

(2) Compared to the only other available $^{230}Th_{xs}$-based IRD flux record, which is in the eastern NA, the western sites experienced much higher IRD flux during all Heinrich events, notably including Heinrich events 3 and 6. We suggest that these two events, in the western North Atlantic at least, were the result of increased ice calving, rather than solely the result of other mechanisms such as increased foraminifera dissolution or reduced productivity.

(3) IRD fluxes during Heinrich events 3 and 6 in the western North Atlantic are smaller than the other typical Heinrich events. This is consistent with the hypothesis that the calving of icebergs from the Laurentide ice sheet increased during H3 and H6 but to a lesser extent than during the other events.

(4) All Heinrich events were accompanied by surface cooling and freshening in the western subpolar North Atlantic.

(5) A series of previously identified cooling events during the last interglacial were found in EW37JPC, which were accompanied with evidence for increased ice rafting that was nevertheless two orders of magnitude smaller than Heinrich events.

(6) We tentatively suggest $(^{230}Th/^{238}U)_{detrital}$ = 0.81 should be used in calculating $^{230}Th_{xs}$ to account for α recoil during the decay and production of both ^{234}U and ^{230}Th, each generating a ~10% loss of the daughter isotope.

(7) Pa/Th reconstruction and interpretation is likely to be particularly challenging in high sediment-flux regions and intervals, as exemplified by the subpolar western North Atlantic during Heinrich events.

Acknowledgements

The authors thank Blanca Alvarez Caraveo for assistance with sample processing, and Kassandra Costa and Martin Fleisher for assistance with U-Th procedure and ICPMS analysis. This research was funded by NSF grant AGS 16-35019. All data needed to evaluate the conclusions in the paper are present in the Supplementary Materials.

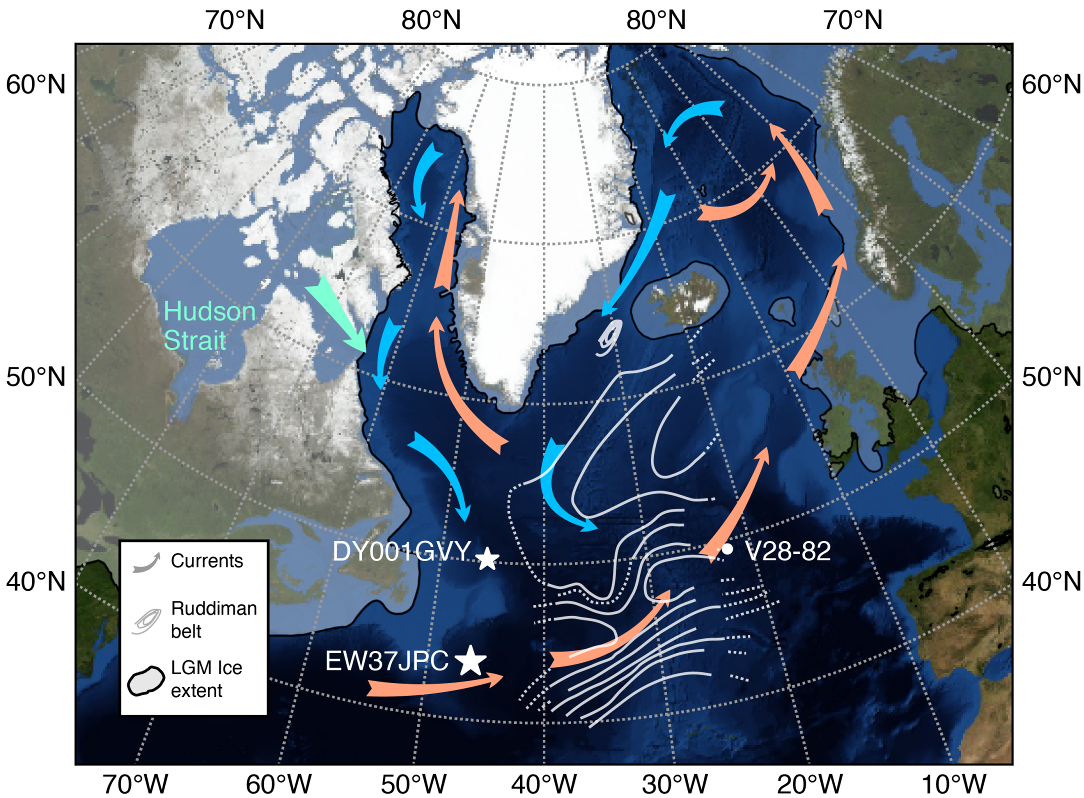

Figure 1. North Atlantic map with core locations. Stars are the cores used by this study: EW37JPC (43°58’N, 46°25’W, 3981m); DY001GVY (50°09’36’’N, 45°30’36’’W, 3721m). White dot is the core used for comparison of IRD flux: V28-82 (49°27’N, 22°16’W, 3935m) (McManus et al., 1998). Frosted area is the ice sheets extent during the Last Glacial Maximum (Ehlers et al., 2011). Red and blue arrows are the warm and cold surface circulation, respectively, after *(Hemming et al., 2002)*. Aqua arrow leaving the Hudson Strait represents the calving of icebergs from the LIS. Contours delineate the Ruddiman IRD belt (Ruddiman, 1977). Basemap from NASA Blue Marble June image (Stockli et al., 2005).

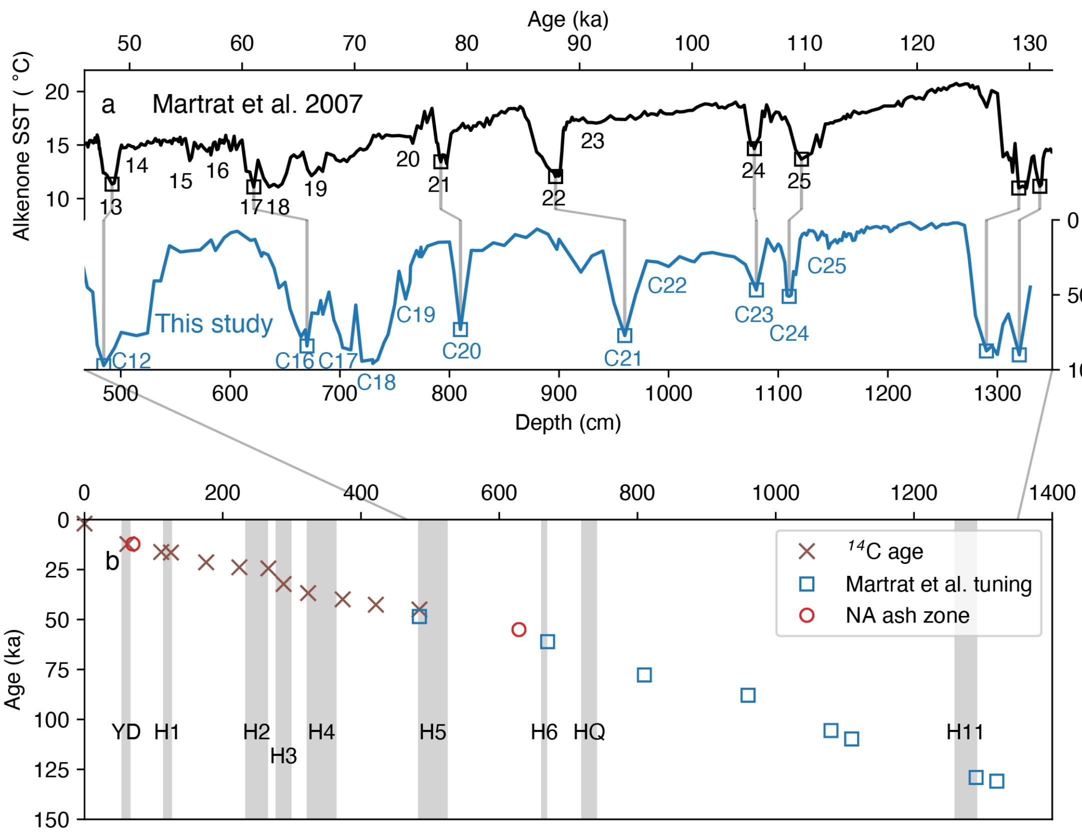

Figure 2. Chronology of EW37JPC. Variations in *N. pachyderma* relative abundance are correlated with an alkenone unsaturation SST record that was previously tied to the North Greenland Ice Core Project (NGRIP) chronology (a) (Martrat et al., 2007; Iberian margin stadials marked in black numbers). Blue numbers denote cooling events (McManus et al., 2002, 1994, see Figure S7 for details). Tie points to our core are marked by thin gray line. The compilation of all age control points, including radiocarbon dating, tephrochronology, and tuning with alkenone record (b).

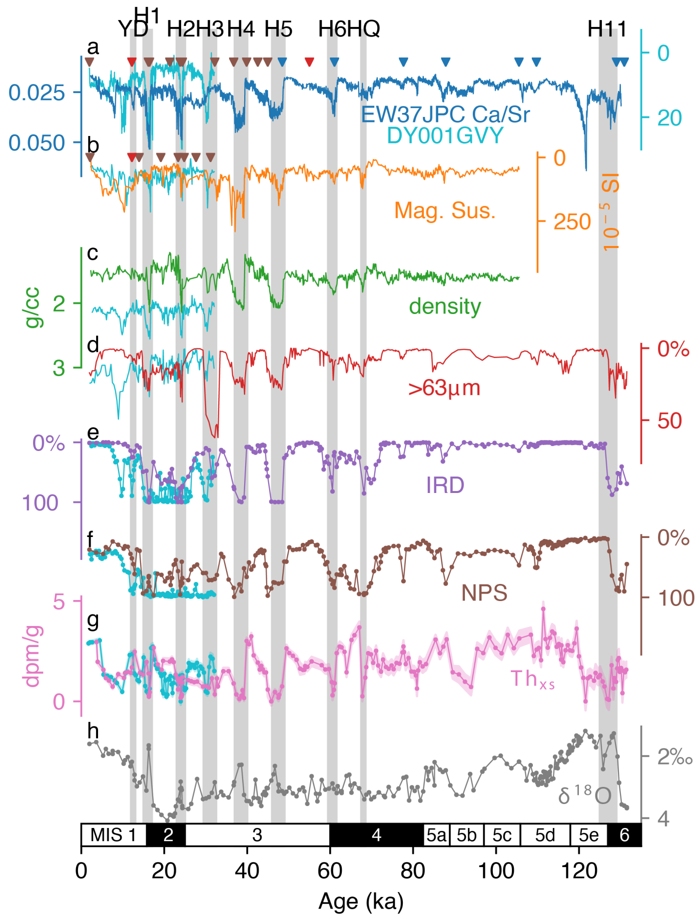

Figure 3. DY001GVY (cyan) and EW37JPC (other colors) Ca/Sr with EW37JPC age control points marked by red (ash zone), brown (radiocarbon), and blue (SST tie points) triangles (a), magnetic susceptibility with DY001GVY age control point marked by red (ash zone) and brown (radiocarbon) triangles (b), bulk wet sediment density (c), coarse (>63µm) fraction (d), IRD abundance (e), *N. pachyderma* abundance, of which the early last interglacial (95-125 ka) data are partially from McManus et al. (2002) (f), $^{230}Th_{xs}$ with shading marking uncertainty (g), and *N. pachyderma* $\delta^{18}O$ (h). Gray bars are Younger Dryas (YD), Heinrich events (H) 1-6, 11, as well as HQ as predicted by Bassis et al. (2017).

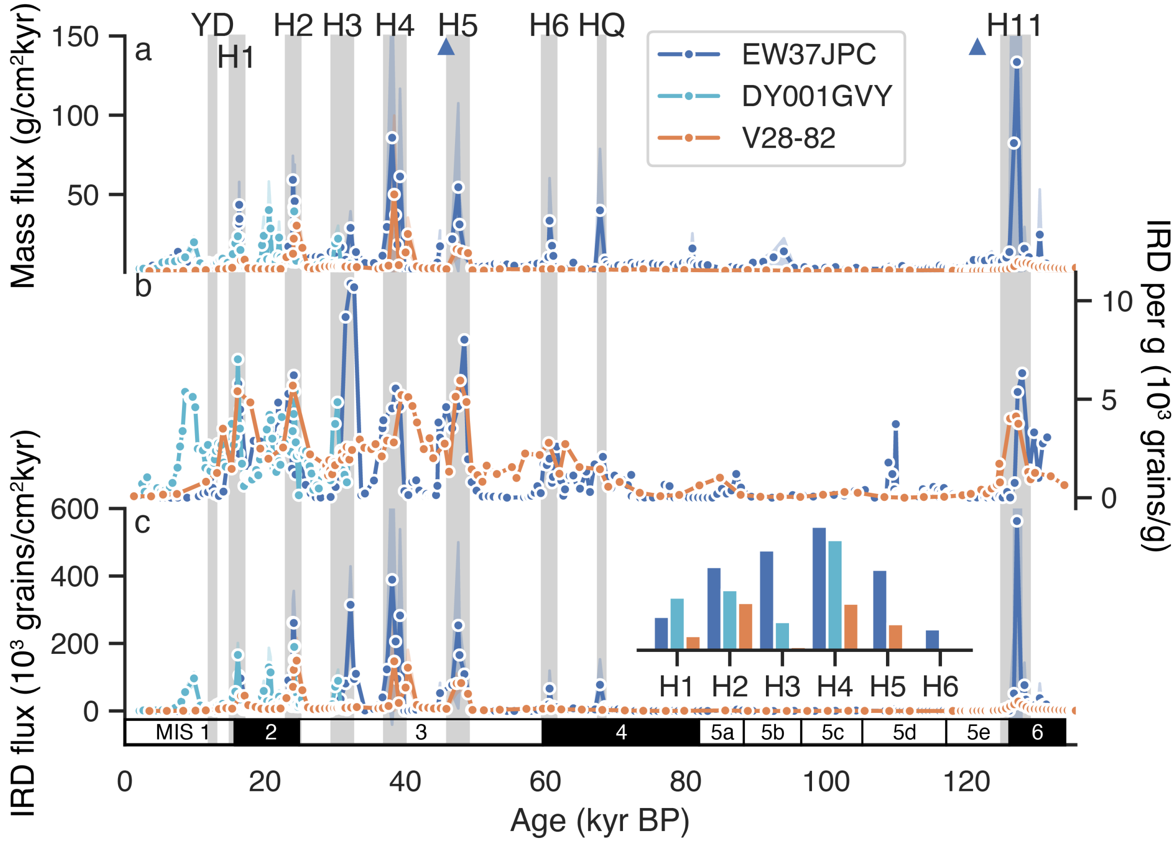

Figure 4. Comparison of EW37JPC, DY001GVY and V28-82 $^{230}Th_{xs}$-normalized mass flux (a), IRD concentration (b), and IRD flux (c). Triangles in (a) are mass flux data points too high to quantify. The inset in (c) compares maximum IRD flux during each Heinrich event relatively.

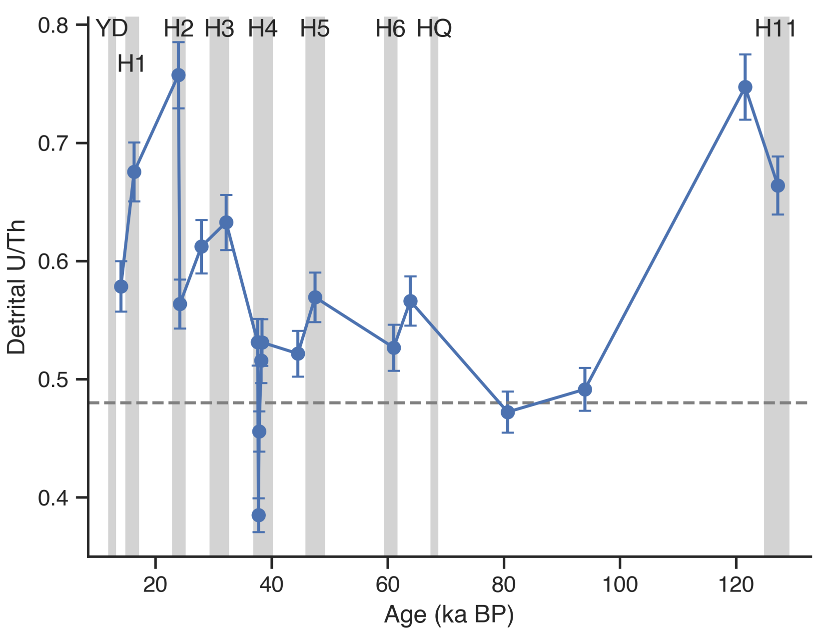

Figure 5. Leaching experiment results from EW37JPC for determining the detrital U/Th ratio. The dashed line is the average ratio (0.48) of the high-resolution measurements within Heinrich event 4, which we use in $^{230}Th_{xs}$ normalization calculations in this study.

Study	**($^{238}U/^{232}Th)_{detrital}$** used
Veiga-Pires and Hillaire-Marcel, 1999	**0.58**
Thomson et al., 1995	**0.67**
Thomson et al., 1999	**0.7**
McManus et al., 2004	**0.57**
Henderson and Anderson, 2003	**0.6**
Böhm et al., 2015	**0.47**
Bourne et al., 2012	**0.55**
Gherardi et al., 2009	**0.6**
Lippold et al., 2009	**0.5**
Lippold et al., 2011	**0.5**
Lippold et al., 2016	**0.6**
Guihou et al., 2010	**0.5**
Guihou et al., 2011	**0.5**
Roberts et al., 2014	**0.6**

Table 1. *Detrital U/Th used by previous studies. The range of the values is 0.47 – 0.7.*

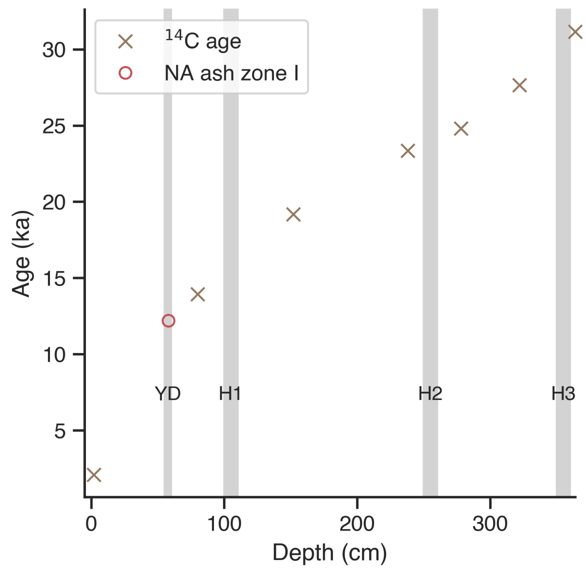

Figure S1. Chronology of DY001GVY.

Figure S2. Turbidite sequence found at 280-290 cm depth in EW37JPC, around the depth of Heinrich layer 3. The distance between the two core depth tags is 10 cm.

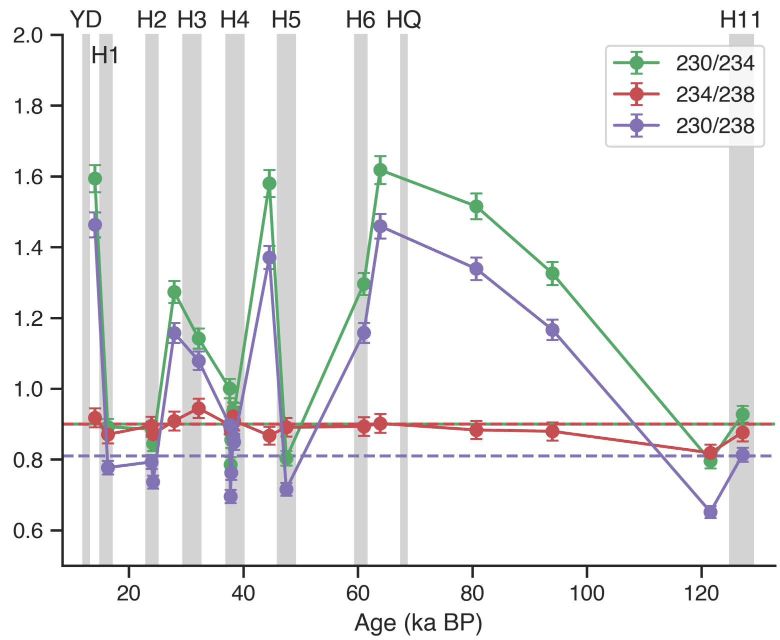

Figure S3. Leaching experiment results from EW37JPC for determining the detrital $^{230}Th/^{238}U$ ratio. Dashed lines are the ratios used by this study (0.9 for $^{230}Th/^{234}U$ and $^{234}U/^{238}U$ and 0.81 for $^{230}Th/^{238}U$).

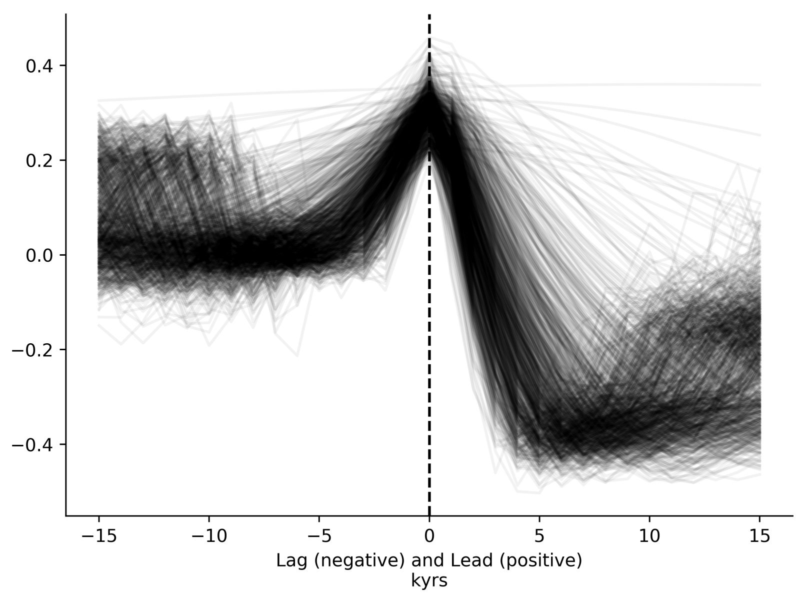

Figure S4. Phasing lag correlations of planktic $\delta^{18}O$ with $^{230}Th_{xs}$ from EW37JPC, bootstrapped 1000 times allowing sampling start time, end time, and time step to vary. Correlation coefficient in the positive (negative) direction is calculated when planktic $\delta^{18}O$ leads (lags) $^{230}Th_{xs}$.

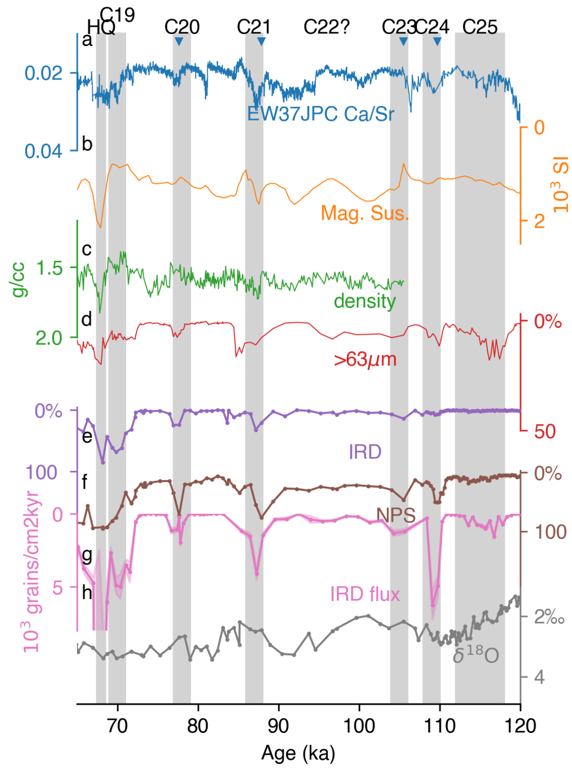

Figure S5. Same as Figure 3 except (g) displays IRD flux and limited to the late last interglacial period for the locally-high IRD flux events from EW37JPC, assigned cooling events numbering according to McManus et al. (1994) and McManus et al. (2002). Shadings are HQ and cooling events.

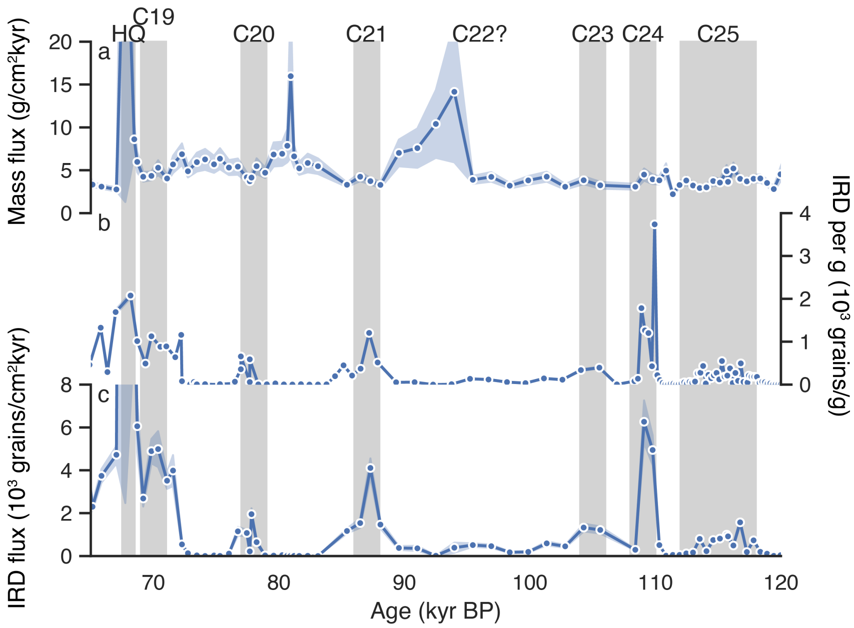

Figure S6. Same as Figure 4 but for the locally-high IRD flux events of the late last interglacial period from EW37JPC, assigned cooling events tentatively according to McManus et al. (1994). Shadings are HQ and cooling events.

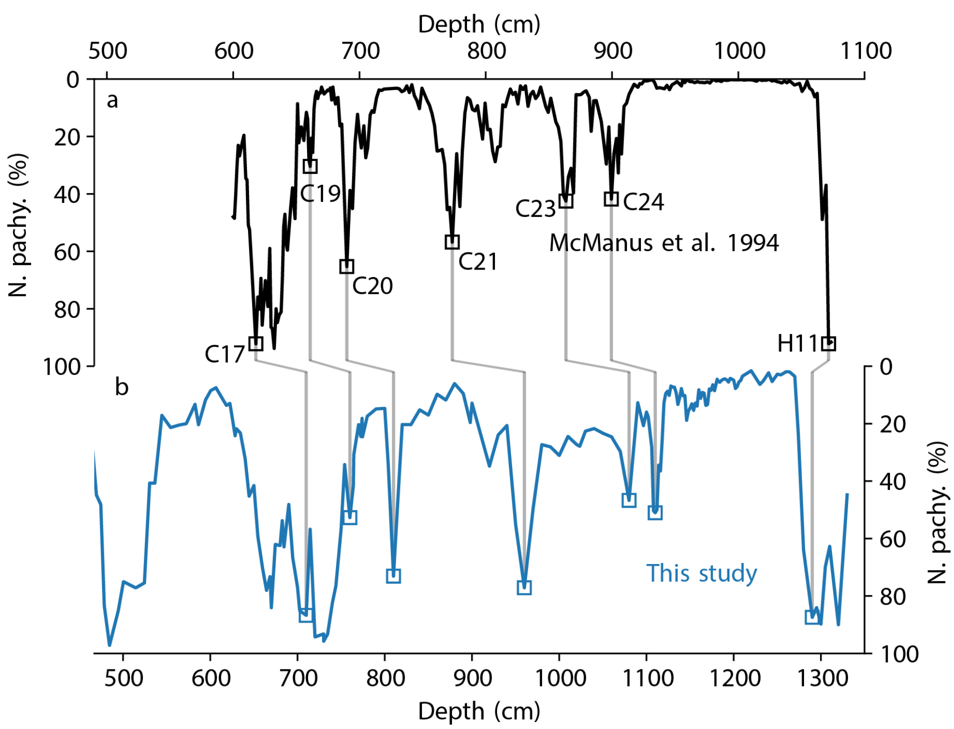

Figure S7. Correlation of last interglacial % *N. pachy.* between EW37JPC and McManus et al. (1994).

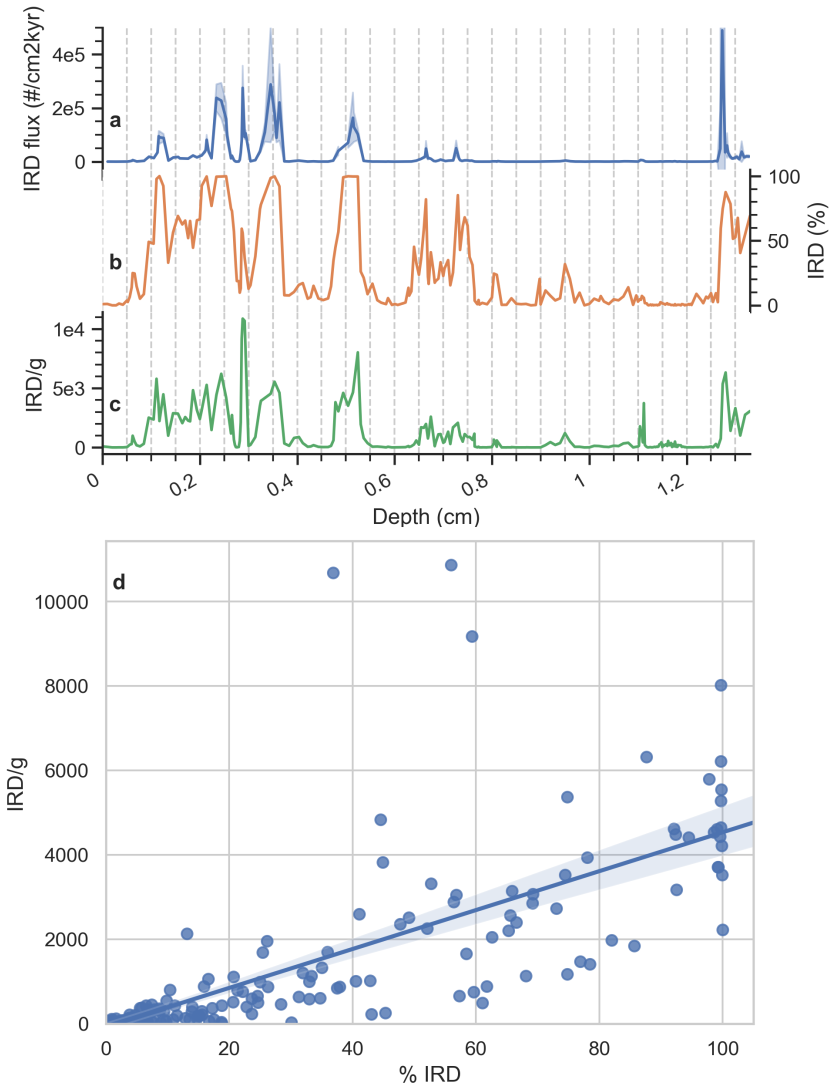

Figure S8. Comparison of three indicators of ice-rafting in EW37JPC: IRD flux (a), % IRD (b), and IRD/g (c). (d) is IRD/g plotted against % IRD. A linear regression line is drawn, as well as the confidence interval (translucent band) calculated from bootstrap (n=1000). The three outliers with >8000 IRD/g are all from Heinrich event 3.

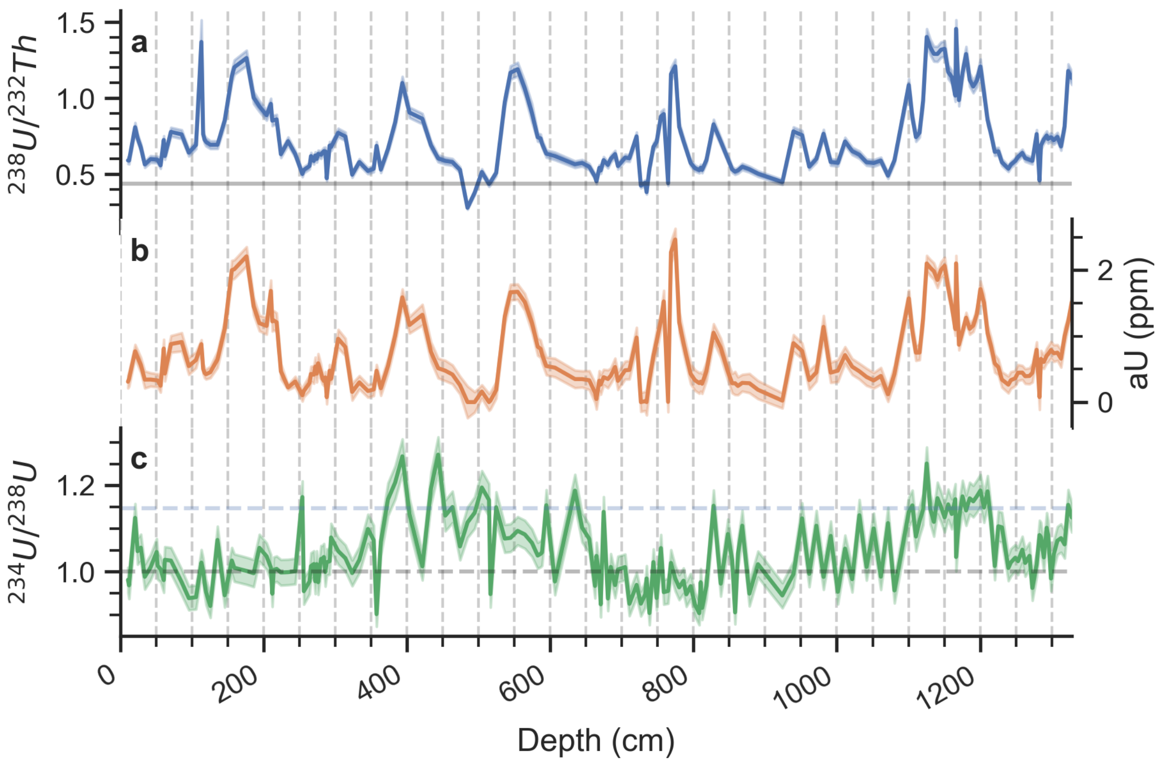

Figure S9. Different proxies of authigenic uranium in EW37JPC. $^{238}U/^{232}Th$ (a), authigenic uranium = $^{238}U-^{232}Th*0.44$ (b), $^{234}U/^{238}U$ (c). The gray line in top panel is the ratio of $(^{238}U/^{232}Th)_{det}$ used by this study. In the bottom panel, blue dashed line is the sea water $^{234}U/^{238}U$ ratio of 1.1468 (Andersen et al., 2010) and gray dash line represents the $^{234}U/^{238}U$ secular equilibrium.

Alley, R.B., Mayewski, P.A., Sowers, T., Stuiver, M., Taylor, K.C., Clark, P.U., 1997. Holocene climatic instability: A prominent, widespread event 8200 yr ago. Geology 25, 483–486.

Alvarez-Solas, J., Charbit, S., Ritz, C., Paillard, D., Ramstein, G., Dumas, C., 2010. Links between ocean temperature and iceberg discharge during Heinrich events. Nature Geoscience 3, 122–126. https://doi.org/10.1038/ngeo752

Alvarez-Solas, J., Robinson, A., Montoya, M., Ritz, C., 2013. Iceberg discharges of the last glacial period driven by oceanic circulation changes. Proceedings of the National Academy of Sciences 110, 16350–16354. https://doi.org/10.1073/pnas.1306622110

Andersen, M.B., Stirling, C.H., Zimmermann, B., Halliday, A.N., 2010. Precise determination of the open ocean $^{234}U/^{238}U$ composition. Geochemistry, Geophysics, Geosystems 11. https://doi.org/10.1029/2010GC003318

Anderson, R.F., Fleisher, M.Q., Lao, Y., 2006. Glacial-interglacial variability in the delivery of dust to the central equatorial Pacific Ocean. Earth and Planetary Science Letters 242, 406–414. https://doi.org/10.1016/j.epsl.2005.11.061

Andrews, J.T., 2000. Icebergs and Iceberg Rafted Detritus (IRD) in the North Atlantic: Facts and Assumptions. Oceanography 13, 100–108. https://doi.org/10.5670/oceanog.2000.19

Andrews, J.T., Voelker, A.H.L., 2018. “Heinrich events” (& sediments): A history of terminology and recommendations for future usage. Quaternary Science Reviews 187, 31–40. https://doi.org/10.1016/j.quascirev.2018.03.017

Bacon, M.P., 1984. Glacial to interglacial changes in carbonate and clay sedimentation in the Atlantic Ocean estimated from ^{230}Th measurements. Chemical Geology 46, 97–111. https://doi.org/10.1016/0009-2541(84)90183-9

Bacon, M.P., Anderson, R.F., 1982. Distribution of thorium isotopes between dissolved and particulate forms in the deep sea. Journal of Geophysical Research 87, 2045. https://doi.org/10.1029/JC087iC03p02045

Bacon, M.P., Rosholt, J.N., 1982. Accumulation rates of Th-230, Pa-231, and some transition metals on the Bermuda Rise. Geochimica et Cosmochimica Acta 46, 651–666. https://doi.org/10.1016/0016-7037(82)90166-1

Bard, E., Rostek, F., Turon, J.L., Gendreau, S., 2000. Hydrological impact of Heinrich events in the subtropical Northeast Atlantic. Science 289, 1321–1324. https://doi.org/10.1126/science.289.5483.1321

Barker, S., Chen, J., Gong, X., Jonkers, L., Knorr, G., Thornalley, D., 2015. Icebergs not the trigger for North Atlantic cold events. Nature 520, 333–336. https://doi.org/10.1038/nature14330

Barker, S., Diz, P., Vautravers, M.J., Pike, J., Knorr, G., Hall, I.R., Broecker, W.S., 2009. Interhemispheric Atlantic seesaw response during the last deglaciation. Nature 457, 1097–1102. https://doi.org/10.1038/nature07770

Barnes, C.E., Cochran, J.K., 1990. Uranium removal in oceanic sediments and the oceanic U balance. Earth and Planetary Science Letters 97, 94–101. https://doi.org/10.1016/0012-821X(90)90101-3

Bassis, J.N., Petersen, S. V., Mac Cathles, L., 2017. Heinrich events triggered by ocean forcing and modulated by isostatic adjustment. Nature 542, 332–334. https://doi.org/10.1038/nature21069

Bond, G., Heinrich, H., Broecker, W., Labeyrie, L., McManus, J., Andrews, J., Huon, S., Jantschik, R., Clasen, S., Simet, C., Tedesco, K., Klas, M., Bonani, G., Ivy, S., 1992.

Evidence for massive discharges of icebergs into the North Atlantic ocean during the last glacial period. Nature 360, 245–249. https://doi.org/10.1038/360245a0

Bond, G.C., Broecker, W.S., Johnsen, S.J., McManus, J.F., Labeyrie, L., Jouzel, J., Bonani, G., 1993. Correlation Between Climate Records From North Altantic Sediments and Greenland Ice. Nature 365, 143–147.

Bourne, M.D., Thomas, A.L., Niocaill, C. Mac, Henderson, G.M., 2012. Improved determination of marine sedimentation rates using $^{230}Th_{xs}$. Geochemistry, Geophysics, Geosystems 13, 1–9. https://doi.org/10.1029/2012GC004295

Broecker, W., Bond, G., Klas, M., Clark, E., McManus, J., 1992. Origin of the northern Atlantic's Heinrich events. Climate Dynamics 6, 265–273. https://doi.org/10.1007/BF00193540

Buizert, C., Sigl, M., Severi, M., Markle, B.R., Wettstein, J.J., McConnell, J.R., Pedro, J.B., Sodemann, H., Goto-Azuma, K., Kawamura, K., Fujita, S., Motoyama, H., Hirabayashi, M., Uemura, R., Stenni, B., Parrenin, F., He, F., Fudge, T.J., Steig, E.J., 2018. Abrupt ice-age shifts in southern westerly winds and Antarctic climate forced from the north. Nature 563, 681–685. https://doi.org/10.1038/s41586-018-0727-5

Cortijo, E., Labeyrie, L., Vidal, L., Vautravers, M., Chapman, M., Duplessy, J.-C., Elliot, M., Arnold, M., Turon, J.-L., Auffret, G., 1997. Changes in sea surface hydrology associated with Heinrich event 4 in the North Atlantic Ocean between 40° and 60°N. Earth and Planetary Science Letters 146, 29–45. https://doi.org/10.1016/S0012-821X(96)00217-8

Costa, K., McManus, J., 2017. Efficacy of ^{230}Th normalization in sediments from the Juan de Fuca Ridge, northeast Pacific Ocean. Geochimica et Cosmochimica Acta 197, 215–225. https://doi.org/10.1016/j.gca.2016.10.034

Dansgaard, W., Johnsen, S.J., Clausen, H.B., Dahl-Jensen, D., Gundestrup, N.S., Hammer, C.U., Hvidberg, C.S., Steffensen, J.P., Sveinbjörnsdóttir, A.E., Jouzel, J., Bond, G.C., Sveinbjörnsdottir, A.E., Jouzel, J., Bond, G.C., 1993. Evidence for general instability of past climate from a 250-kyr ice-core record. Nature 364, 218–220. https://doi.org/10.1038/364218a0

Death, R., Siegert, M.J., Bigg, G.R., Wadley, M.R., 2006. Modelling iceberg trajectories, sedimentation rates and meltwater input to the ocean from the Eurasian Ice Sheet at the Last Glacial Maximum. Palaeogeography, Palaeoclimatology, Palaeoecology 236, 135–150. https://doi.org/10.1016/j.palaeo.2005.11.040

DePaolo, D.J., Maher, K., Christensen, J.N., McManus, J., 2006. Sediment transport time measured with U-series isotopes: Results from ODP North Atlantic drift site 984. Earth and Planetary Science Letters 248, 379–395. https://doi.org/10.1016/j.epsl.2006.06.004

Ehlers, J., Ehlers, Jürgen, Gibbard, P.L., Hughes, P.D., 2011. Quaternary Glaciations - Extent and Chronology: A Closer Look. Elsevier.

Ellison, C.R.W., Chapman, M.R., Hall, I.R., 2006. Surface and Deep Ocean Interactions During the Cold Climate Event 8200 Years Ago. Science 312, 1929–1932. https://doi.org/10.1126/science.1127213

EPICA Community Members, 2004b. Eight glacial cycles from an Antarctic ice core. Nature 429, 623–628. http://dx.doi.org/10.1038/nature02599

Ericson, D.B.., 1959. Coiling Direction of Globigerina pachyderma as a Climatic Index. Science 130, 219–220.

Fleisher, M.Q., Anderson, R.F., 1991. Particulate matter digestion (From Mg to 10’s Of G) and radionuclide blanks. Geophysical Monograph Series 63, 221–222.

Francois, R., Bacon, M.P., Suman, D.O., 1990. Thorium 230 profiling in deep-sea sediments: high-resolution records of flux and dissolution of carbonate in the equatorial Atlantic during the last 24,000 years. Paleoceanography 5, 761–787. https://doi.org/0883-8305/90/90PA-016

Francois, R., Frank, M., Rutgers van der Loeff, M.M., Bacon, M.P., 2004. ^{230}Th normalization: An essential tool for interpreting sedimentary fluxes during the late Quaternary. Paleoceanography 19, PA1018. https://doi.org/10.1029/2003PA000939

Ganopolski, A., Rahmstorf, S., 2001. Rapid changes of glacial climate simulated in a coupled climate model. Nature 409, 153–158. https://doi.org/10.1038/35051500

Grootes, P.M., Stuiver, M., White, J.W.C., Johnsen, S., Jouzel, J., 1993. Comparison of oxygen isotope records from the GISP2 and GRIP Greenland ice cores. Nature 366, 552.

Grousset, F.E., Labeyrie, L., Sinko, J.A., Bond, G., Duprat, J., Cortijo, E., Cremer, M., Bond, G., Duprat, J., Cortijo, E., Huon, S., 1993. Patterns of Ice-Rafted Detritus in the Glacial North Atlantic (40-55°N). Paleoceanography 8, 175–192. https://doi.org/10.1029/92PA02923

Grousset, F.E., Pujol, C., Labeyrie, L., Auffret, G., A. Boelaert, A., 2000. Were the North Atlantic Heinrich events triggered by the behaviour of the European ice sheets? Geology 28, 123–126. https://doi.org/10.1130/0091-7613(2000)28<123:WTNAHE>2.0.CO;2

Gwiazda, R.H., Hemming, S.R., Broecker, W.S., 1996. Provenance of icebergs during Heinrich Event 3 and the contrast to their sources during other Heinrich episodes. Paleoceanography 11, 371–378. https://doi.org/10.1029/96PA01022

Heinrich, H., 1988. Origin and consequences of cyclic ice rafting in the Northeast Atlantic Ocean during the past 130,000 years. Quaternary Research 29, 142–152. https://doi.org/10.1016/0033-5894(88)90057-9

Hemming, S.R., 2004. Heinrich events: Massive late Pleistocene detritus layers of the North Atlantic and their global climate imprint. Reviews of Geophysics 42, 1–43. https://doi.org/10.1029/2003RG000128.1.INTRODUCTION

Hemming, S.R., Hall, C.M., Biscaye, P.E., Higgins, S.M., Bond, G.C., McManus, J.F., Barber, D.C., Andrews, J.T., Broecker, W.S., 2002. $^{40}Ar/^{39}Ar$ ages and $^{40}Ar^*$ concentrations of fine-grained sediment fractions from North Atlantic Heinrich layers. Chemical Geology 182, 583–603. https://doi.org/10.1016/S0009-2541(01)00342-4

Henry, L.G., Mcmanus, J.F., Curry, W.B., Roberts, N.L., Piotrowski, A.M., Keigwin, L.D., 2016. North Atlantic ocean circulation and abrupt climate change during the last glaciation. Science 353, 470–474. https://doi.org/10.1126/science.aaf5529

Hillaire-Marcel, C., Vernal, A. de, Bilodeau, G., Wu, G., 1994. Isotope stratigraphy, sedimentation rates, deep circulation, and carbonate events in the Labrador Sea during the last ~200 ka. Can. J. Earth Sci. 31, 63–89. https://doi.org/10.1139/e94-007

Hodell, D.A., Channeil, J.E.T., Curtis, J.H., Romero, O.E., Röhl, U., 2008. Onset of “Hudson Strait” Heinrich events in the eastern North Atlantic at the end of the middle Pleistocene transition (~640 ka)? Paleoceanography 23, 1–16. https://doi.org/10.1029/2008PA001591

Johnsen, S.J., Clausen, H.B., Dansgaard, W., Fuhrer, K., Gundestrup, N.S., Hammer, C.U., Iversen, P., Jouzel, J., Stauffer, B., Steffensen, J.P., 1992. Irregular glacial interstadials recorded in a new Greenlan ice core. Nature 359, 311. https://doi.org/10.1038/350055a0

Johnsen, S.J., Dahl-Jensen, D., Gundestrup, N., Steffensen, J.P., Clausen, H.B., Miller, H., Masson-Delmotte, V., Sveinbjörnsdottir, A.E., White, J., 2001. Oxygen isotope and palaeotemperature records from six Greenland ice-core stations: Camp Century, Dye-3, GRIP, GISP2, Renland and NorthGRIP. Journal of Quaternary Science 16, 299–307. https://doi.org/10.1002/jqs.622

Jullien, E., Grousset, F.E., Hemming, S.R., Peck, V.L., Hall, I.R., Jeantet, C., Billy, I., 2006. Contrasting conditions preceding MIS3 and MIS2 Heinrich events. Global and Planetary Change 54, 225–238. https://doi.org/10.1016/j.gloplacha.2006.06.021

Keigwin, L.D., Sachs, J.P., Rosenthal, Y., Boyle, E.A., 2005. The 8200 year B.P. event in the slope water system, western subpolar North Atlantic. Paleoceanography 20. https://doi.org/10.1029/2004PA001074

Kirby, E., Andrews, T., 1999. Mid-Wisconsin Laurentide Ice Sheet growth and decay: Implications for Heinrich events 3 and 4. Paleoceanography 14, 211–223.

Klinkhammer, G.P., Palmer, M.R., 1991. Uranium in the oceans: Where it goes and why. Geochimica et Cosmochimica Acta 55, 1799–1806. https://doi.org/10.1016/0016-7037(91)90024-Y

Labeyrie, L., Leclaire, H., Waelbroeck, C., Cortijo, E., Duplessy, J.-C., Vidal, L., Elliot, M., Coat, B.L., Auffret, G., 1999. Temporal Variability of the Surface and Deep Waters of the North West Atlantic Ocean at Orbital and Millennial Scales, in: Mechanisms of Global Climate Change at Millennial Time Scales. American Geophysical Union (AGU), pp. 77–98. https://doi.org/10.1029/GM112p0077

Lao, Y., Anderson, R.F., Broecker, W.S., Hofmann, H.J., Wolfli, W., 1993. Particulate fluxes of ^{230}Th, ^{231}Pa, and ^{10}Be in the northeastern Pacific Ocean. Geochimica et Cosmochimica Acta 57, 205–217. https://doi.org/10.1016/0016-7037(93)90479-G

Manabe, S., Stouffer, R.J., 1997. Coupled ocean-atmosphere model response to freshwater input: Comparison to Younger Dryas Event. Paleoceanography 12, 321–336. https://doi.org/10.1029/96PA03932

Marcott, S.A., Clark, P.U., Padman, L., Klinkhammer, G.P., Springer, S.R., Liu, Z., Otto-Bliesner, B.L., Carlson, A.E., Ungerer, A., Padman, J., He, F., Cheng, J., Schmittner, A., 2011. Ice-shelf collapse from subsurface warming as a trigger for Heinrich events. Proceedings of the National Academy of Sciences 108, 13415–13419. https://doi.org/10.1073/pnas.1104772108

Marshall, S.J., Koutnik, M.R., 2006. Ice sheet action versus reaction: Distinguishing between Heinrich events and Dansgaard-Oeschger cycles in the North Atlantic. Paleoceanography 21, 1–13. https://doi.org/10.1029/2005PA001247

Martrat, B., Grimalt, J.O., Shackleton, N.J., de Abreu, L., Hutterli, M.A., Stocker, T.F., 2007. Four Climate Cycles of Recurring Deep and Surface Water Destabilizations on the Iberian Margin. Science 317, 502–507. https://doi.org/10.1126/science.1139994

McCartney, M., 1992. Recirculating components to the deep boundary current of the northern North Atlantic. Progress in Oceanography 29, 283–383.

McManus, J.F., Anderson, R.F., Broecker, W.S., Fleisher, M.Q., Higgins, S.M., 1998. Radiometrically determined sedimentary fluxes in the sub-polar North Atlantic during the last 140,000 years. Earth and Planetary Science Letters 155, 29–43. https://doi.org/10.1016/S0012-821X(97)00201-X

McManus, J.F., Bond, G.C., Broecker, W.S., Johnsen, S., Labeyrie, L., Higgins, S., 1994. High-resolution climate records from the North Atlantic during the last interglacial. Nature 371, 326–329. https://doi.org/10.1038/371326a0

McManus, J.F., Francois, R., Gherardi, J.-M., Keigwin, L.D., Brown-Leger, S., 2004. Collapse and rapid resumption of Atlantic meridional circulation linked to deglacial climate changes. Nature 428, 834–837. https://doi.org/10.1038/nature02494

McManus, J.F., Oppo, D.W., Keigwin, L.D., Cullen, J.L., Bond, G.C., 2002. Thermohaline Circulation and Prolonged Interglacial Warmth in the North Atlantic. Quaternary Research 58, 17–21. https://doi.org/10.1006/qres.2002.2367

Missiaen, L., Pichat, S., Waelbroeck, C., Douville, E., Bordier, L., Dapoigny, A., Thil, F., Foliot, L., Wacker, L., 2018. Downcore Variations of Sedimentary Detrital ($^{238}U/^{232}Th$) Ratio: Implications on the Use of 230Thxs and 231Paxs to Reconstruct Sediment Flux and Ocean Circulation. Geochemistry, Geophysics, Geosystems 19, 2560–2573. https://doi.org/10.1029/2017GC007410

Murray, R.W., Miller, D.J., Kryc, K.A., 2000. Analysis of major and trace elements in rocks, sediments, and interstitial waters by inductively coupled plasma-atomic emission spectrometry (ICP-AES). ODP Tech. Note.

Naafs, B.D.A., Hefter, J., Ferretti, P., Stein, R., Haug, G.H., 2011. Sea surface temperatures did not control the first occurrence of Hudson Strait Heinrich Events during MIS 16. Paleoceanography 26, 1–10. https://doi.org/10.1029/2011PA002135

NGRIP members, 2004. High-resolution record of Northern Hemisphere climate extending into the last interglacial period. Nature 431, 147–151. https://doi.org/10.1038/nature02805

Parrenin, F., Rémy, F., Ritz, C., Siegert, M.J., Jouzel, J., 2004. New modeling of the Vostok ice flow line and implication for the glaciological chronology of the Vostok ice core. Journal of Geophysical Research D: Atmospheres 109. https://doi.org/10.1029/2004JD004561

Peck, V.L., Hall, I.R., Zahn, R., Grousset, F., Hemming, S.R., Scourse, J.D., 2007. The relationship of Heinrich events and their European precursors over the past 60 ka BP: a multi-proxy ice-rafted debris provenance study in the North East Atlantic. Quaternary Science Reviews 26, 862–875. https://doi.org/10.1016/j.quascirev.2006.12.002

Prange, M., Lohmann, G., Romanova, V., Butzin, M., 2004. Modelling tempo-spatial signatures of Heinrich Events: influence of the climatic background state. Quaternary Science Reviews 23, 521–527. https://doi.org/10.1016/j.quascirev.2003.11.004

Rahmstorf, S., 1995. Bifurcations of the Atlantic thermohaline circulation in response to changes in the hydrological cycle. Nature 378, 145. https://doi.org/10.1038/378145a0

Rashid, H., Hesse, R., Piper, D.J.W., 2003. Evidence for an additional Heinrich event between H5 and H6 in the Labrador Sea. Paleoceanography 18, 1–15. https://doi.org/10.1029/2003PA000913

Rashid, H., Saint-Ange, F., Barber, D.C., Smith, M.E., Devalia, N., 2012. Fine scale sediment structure and geochemical signature between eastern and western North Atlantic during Heinrich events 1 and 2. Quaternary Science Reviews 46, 136–150. https://doi.org/10.1016/j.quascirev.2012.04.026

Rasmussen, S.O., Andersen, K.K., Svensson, A.M., Steffensen, J.P., Vinther, B.M., Clausen, H.B., Siggaard-Andersen, M.L., Johnsen, S.J., Larsen, L.B., Dahl-Jensen, D., Bigler, M., Röthlisberger, R., Fischer, H., Goto-Azuma, K., Hansson, M.E., Ruth, U., 2006. A new

Greenland ice core chronology for the last glacial termination. Journal of Geophysical Research Atmospheres 111, 1–16. https://doi.org/10.1029/2005JD006079

Roberts, W.H.G., Valdes, P.J., Payne, A.J., 2014. A new constraint on the size of Heinrich Events from an iceberg/sediment model. Earth and Planetary Science Letters 386, 1-9, https://doi.org/10.1016/j.epsl.2013.10.020

Robinson, L.F., Noble, T.L., McManus, J.F., 2008. Measurement of adsorbed and total 232Th/230Th ratios from marine sediments. Chemical Geology 252, 169–179. https://doi.org/10.1016/j.chemgeo.2008.02.015

Roche, D., Paillard, D., Cortijo, E., 2004. Constraints on the duration and freshwater release of Heinrich event 4 through isotope modelling. Nature 432, 379–382. https://doi.org/10.1038/nature03059

Rodrigues, T., Alonso-García, M., Hodell, D.A., Rufino, M., Naughton, F., Grimalt, J.O., Voelker, A.H.L., Abrantes, F., 2017. A 1-Ma record of sea surface temperature and extreme cooling events in the North Atlantic: A perspective from the Iberian Margin. Quaternary Science Reviews 172, 118–130. https://doi.org/10.1016/j.quascirev.2017.07.004

Ruddiman, W.F., 1977. North Atlantic Ice-Rafting: A Major Change at 75,000 Years Before the Present. Science (New York, N.Y.) 196, 1208–1211. https://doi.org/10.1126/science.196.4295.1208

Ruddiman, W.F., Glover, L.K., 1972. Vertical mixing of Ice-rafted volcanic Ash in North Atlantic Sediments. Geological Society of America Bulletin 83, 2817–2836.

Snoeckx, H., Grousset, F., Revel, M., Boelaert, A., 1999. European contribution of ice-rafted sand to Heinrich layers H3 and H4. Marine Geology 158, 197–208. https://doi.org/10.1016/S0025-3227(98)00168-6

Southon, J., 2004. A Radiocarbon Perspective on Greenland Ice-Core Chronologies: Can we Use Ice Cores for 14C Calibration? Radiocarbon 46, 1239–1259. https://doi.org/10.1017/S0033822200033129

Stein, R., Hefter, J., Grützner, J., Voelker, A., David A Naafs, B., 2009. Variability of surface water characteristics and Heinrich-like events in the Pleistocene midlatitude North Atlantic Ocean: biomarker and XRD records from IODP site U1313 (MIS 16-9). Paleoceanography 24, 1–13. https://doi.org/10.1029/2008PA001639

Stockli, R., Vermote, E., Saleous, N., Simmon, R., Herring, D., 2005. The Blue Marble Next Generation - A true color earth dataset including seasonal dynamics from MODIS.

Stuiver, M., Reimer, P.J., Reimer, R.W., 2019. CALIB 7.1 [WWW program].

Svensson, A., Andersen, K.K., Bigler, M., Clausen, H.B., Dahl-Jensen, D., Davies, S.M., Johnsen, S.J., Muscheler, R., Parrenin, F., Rasmussen, S.O., Röthlisberger, R., Seierstad, I., Steffensen, J.P., Vinther, B.M., 2008. A 60 000 year Greenland stratigraphic ice core chronology. Climate of the Past 4, 47–57. https://doi.org/10.5194/cp-4-47-2008

Valletta, R.D., Willenbring, J.K., Passchier, S., Elmi, C., 2018. ^{10}Be/ ^{9}Be Ratios Reflect Antarctic Ice Sheet Freshwater Discharge During Pliocene Warming. Paleoceanography and Paleoclimatology. https://doi.org/10.1029/2017PA003283